Tuning and Maximizing the Single-Molecule Surface-Enhanced Raman Scattering from DNA-Tethered Nanodumbbells

Jung-Hoon Lee,[†] Jwa-Min Nam,[*,†] Ki-Seok Jeon,[‡] Dong-Kwon Lim,[†] Hyoki Kim,[§] Sunghoon Kwon,[§] Haemi Lee,[‡] and Yung Doug Suh[*,‡]

[†]Department of Chemistry and [§]School of Electrical Engineering and Computer Science & Inter-University Semiconductor Research Center (ISRC), Seoul National University, Seoul 151-747, South Korea and [‡]Laboratory for Advanced Molecular Probing (LAMP), NanoBio Fusion Research Center, Korea Research Institute of Chemical Technology, DaeJeon 305-600, South Korea

ABSTRACT We extensively study the relationships between single-molecule surface-enhanced Raman scattering (SMSERS) intensity, enhancement factor (EF) distribution over many particles, interparticle distance, particle size/shape/composition and excitation laser wavelength using the single-particle AFM-correlated Raman measurement method and theoretical calculations. Two different single-DNA-tethered Au—Ag core—shell nanodumbbell (GSND) designs with an engineerable nanogap were used in this study: the GSND-I with various interparticle nanogaps from ~4.8 nm to <1 nm or with no gap and the GSND-II with the fixed interparticle gap size and varying particle size from a 23—30 nm pair to a 50—60 nm pair. From the GSND-I, we learned that synthesizing a <1 nm gap is a key to obtain strong SMSERS signals with a narrow EF value distribution. Importantly, in the case of the GSND-I with <1 nm interparticle gap, an EF value of as high as 5.9×10^{13} (average value = 1.8×10^{13}) was obtained and the EF values of analyzed particles were narrowly distributed between 1.9×10^{12} and 5.9×10^{13}. In the case of the GSND-II probes, a combination of >50 nm Au cores and 514.5 nm laser wavelength that matches well with Ag shell generated stronger SMSERS signals with a more narrow EF distribution than <50 nm Au cores with 514.5 nm laser or the GSND-II structures with 632.8 nm laser. Our results show the usefulness and flexibility of these GSND structures in studying and obtaining SMSERS structures with a narrow distribution of high EF values and that the GSNDs with < 1 nm are promising SERS probes with highly sensitive and quantitative detection capability when optimally designed.

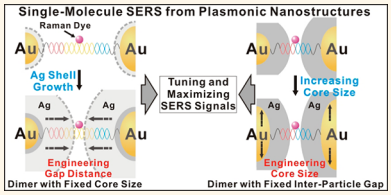

KEYWORDS: surface-enhanced Raman scattering · single-molecule detection · nanogap · core—shell particle · enhancement factor · plasmonic probe

Developing and studying the surface-enhanced Raman scattering (SERS)-active nanostructures for highly sensitive molecular detection have been of great interest to many researchers since single-molecule SERS (SMSERS) was first reported in 1997.[1−9] Typically, the SERS-active nanostructures contain the "hot-spot" regions, typically formed within the gap between plasmonic nanoparticles, and the distance and structural/chemical details between particles along with particle size, shape, and composition are known to play important roles in SERS.[10−17] This hot plasmonic junction can induce a strong electromagnetic field enhancement and also drastically amplify the Raman scattering signal by a factor of many orders of magnitude.[16] However, the more complete and better understanding of this plasmonic coupling with respect to controlling the magnitude and distribution of the enhancement factors (EFs) based on the reliable data is limited due to the lack of the high-yield synthetic methods of the targeted plasmonic nanostructures with nanometer or subnanometer precision and high structural reproducibility. It is especially important to control a <1 nm plasmonic gap because the plasmonic coupling intensity increases exponentially within a <1 nm gap formed between plasmonic nanoparticles such as Au and Ag nanoparticles (AuNPs and AgNPs).[3,18] Although very high EF values up to 10^{13} or 10^{14} have been reported, it was shown that an EF value of 10^{7} to 10^{8} may be large enough even for single-molecule detection, and more important issues are to synthesize the hot SERS nanostructures with high structural reproducibility on the nanometer scale and to obtain a narrow distribution of the high EF values in a reliable fashion.[19−24] Various synthetic and fabrication methods generate nanoparticle-based clusters, and plasmonic nanogaps are formed *via* salt-induced colloidal agglomeration,[25−27] thiol linker-based gold clusters,[28] dimers or multimers using

* Address correspondence to jmnam@snu.ac.kr, ydsuh@krict.re.kr.

Received for review June 26, 2012 and accepted October 4, 2012.

Published online October 04, 2012
10.1021/nn3028216

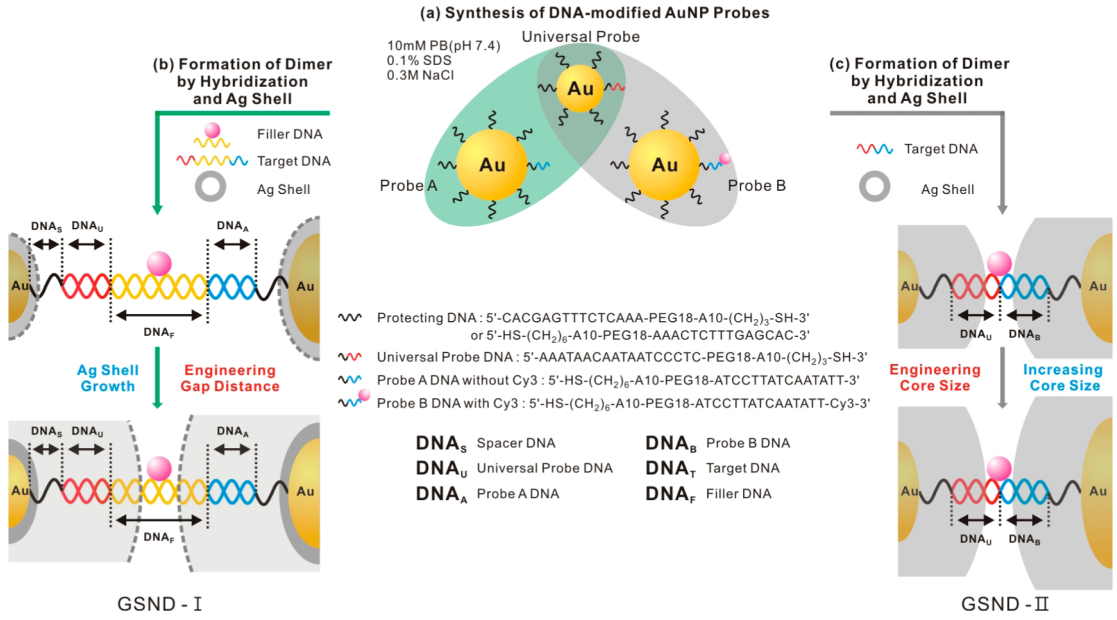

Figure 1. Schematic illustration of DNA sequences and two different DNA-tethered gold–silver nanodumbbell probe designs for the plasmonic nanogap-based single-molecule SERS studies.

functional organic molecules,[29,30] polymer encapsulation,[31,32] hybridization of DNA-modified gold nanoparticles,[33,34] particle etching,[35] electrostatic control,[36] self-assembly of polymer film[37] or a lithographic technique.[38] However, the SERS-based single-molecule detection is still controversial with respect to practicality in use and reliability in data, and a controllable <1 nm plasmonic gap is often needed to generate the ultrahigh EF values with reproducibility and to detect a Raman signal from a single molecule. One other note is that the SERS provides the narrow spectral lines with the unique fingerprint peaks that could make possible for the multiplexed detection of various biomolecules.[39,40] Moreover, it is well-known that the surface-enhanced resonance Raman scattering (SERRS) effect could further amplify Raman signals when the illuminated laser wavelength is resonant with the excitation of dyes.[39–41] Therefore, combining this enormous signal amplification from SERS with resonant dyes, which could induce the resonance effect, offers the possibility of developing ultrasensitive and multiplexed biodetection methods with SERS.

Recently, we reported a high-yield synthetic method for preparing the SERS-active dimeric gold–silver core–shell nanodumbbells (GSNDs), tethered with a single DNA, and it was shown that the nanogap between two particles can be engineered on the nanometer scale with silver nanoshell for detecting a single DNA with a single nanodumbbell structure from the SERS signal.[42] It is critical to understand which structural or measurement parameters are important and to control these parameters for obtaining highly amplified and quantifiable SERS signals. However, neither strategic probe design nor systematic study results on the relationships between change in the GSND structure and the EF value from each GSND have been shown therein. The important parameters in this plasmonic nanogap structure include DNA length, nanogap distance, Au core size, Ag shell thickness, and excitation laser wavelength. Understanding and utilizing the relationships between these parameters and the SERS signal could greatly increase our knowledge about the SERS, give insights in designing and synthesizing the SERS nanoprobes and show a direction in generating and measuring the SERS signals from these nanostructures. It should be noted that the DNA-modified Au–Ag core–shell nanostructures are powerful and useful because this combines the high chemical stability of DNA–AuNPs with the strong optical properties of a Ag nanoshell. Recently, it was further shown that Au–Ag core–shell nanoparticles can be potentially used as ratiometric sensors with a very wide dynamic range because the plasmon resonances of the near-spherical core–shell nanoparticles heavily depend on the relative size of the core and shell.[43]

Here, we newly designed and synthesized single DNA-tethered GSND probes to systematically explore the relationships between SERS signal/enhancement factor and nanodumbbell composition, shell thickness, core–metal size, DNA length, or excitation laser wavelength to generate a narrow distribution of higher EF values for higher signal intensity and better signal reproducibility using the single-particle Raman signal measurement method and three-dimensional finite-element-method (3D FEM) calculation (Figure 1). DNA is an emerging functional group that can be used as a promising template for assembly of nanostructures in a programmable way due to their specific Watson–Crick

base pairing and 3D structural features. In forming dimeric GSND structures, we introduced three different DNA sequence designs: protecting DNA for particle stabilization, probe DNA for specific target DNA hybridization, and filler DNA for filling the unhybridized DNA region (Figure 1). After forming the dimeric structures by DNA hybridization, the silver nanoshell formation to engineer the nanogap between AuNPs was followed. Filler DNA approach is useful in synthesizing a wider interparticle gap and positioning one Raman dye in the nanogap for single-molecule detection because synthesizing and purifying very long oligonucleotides are highly challenging. For all the SERS experiments, we used the AFM-correlated nano-Raman spectroscope for obtaining the signals from individual particles.[42,44] With the GSND-I structures, we found that the SERS signal was extremely sensitive to the interparticle nanogap distance and the maximum EF value of 5.9×10^{13} with an average value of 1.8×10^{13} was observed with <1 nm internanogap. The results show that the degree of enhancement becomes much more significant due to an extraordinarily strong plasmonic coupling when interparticle gap distance becomes <1 nm.[12,13] Significantly, for <1 nm interparticle gap particles, a narrow distribution of very high EF values was obtained. However, when two particles are in contact with each other, the EF values get smaller again and a very wide EF distribution was observed. These results show controlling the interparticle gap at a subnanometer level is a key to obtaining the strong and quantifiable SERS signals from plasmonic nanogap structures. The GSND-II results showed that, in general, the intensity of SERS signal was increased as the relative Au composition over Ag composition and overall particle size increase. With respect to the excitation laser wavelength dependence, the results from both experiment and 3D FEM calculation showed more enhanced EF values were obtained with 514.5 nm excitation laser than with the 632.8 nm excitation laser. The results suggest that the relative volume between Au and Ag could affect their plasmon resonance energy and choosing a proper laser wavelength is a key to generating higher and stronger SMSERS signals. The synthetic strategies for the GSNDs and bimetallic interparticle plasmonic coupling-based SERS results reported herein could provide flexible synthetic platforms in constructing various SERS-active nanogap structures and offer insight and optimized probe parameters in obtaining more sensitive and quantifiable SERS results from plasmonic nanogap probes.

RESULTS AND DISCUSSION

In the preparation of single DNA-tethered Au nanodumbbells, two types of nanodumbbells were formed. The Au nanodumbell-I with a wider interparticle nanogap between AuNPs was formed *via* the recognition of longer target DNA and subsequent hybridization of Raman-dye-modified filler DNA (a and b in Figure 1). The Au nanodumbbell-II with a narrower interparticle nanogap between AuNPs was formed *via* a shorter target DNA hybridization (a and c in Figure 1). In a typical experiment, the nanoparticle assembly process was started with the modification of a single thiolated DNA to an AuNP. Having ~1 probe DNA per probe is important because our goals are synthesizing AuNP dimers in a high yield *via* single target DNA hybridization and measuring the single-molecule Raman spectrum.[42] The loading number of DNA per particle was decided based on quantification *via* a fluorescence spectrum measurement. On the basis of the DNA loading number, we controlled the numbers of probe DNA and protecting DNA stoichiometrically (see the Supporting Information and method for experimental details). For the hybridization of DNA−AuNPs to form a GSND with an extended distance between AuNPs (GSND-I), we used a longer target DNA sequence and the filler DNA sequence (denoted as DNA_F; see the filler recognition region in Figure 1). In our case, 31mer DNA_F with a Cy3 dye was hybridized between the universal probe DNA (DNA_U) for 20 nm AuNP and the probe A DNA (DNA_A) for 30 nm AuNP after linking these two particles with target DNA. By filling the unhybridized DNA region with a Cy3-modified DNA_F, a higher structural rigidity and a more stretched DNA form can be obtained and a single Raman dye can be more precisely located at the center between two particles. By using this strategy, we can fabricate a wide range of interparticle gap distances and Ag shell thicknesses, and this allows for studying the distance-dependent SERS effect more systematically and thoroughly as compared to our previous probe design.[42] For the synthetic details of the GSND particles and various Ag shell formations, please see the Supporting Information and Methods section.

The syntheses of the GSND-I particles with various Ag shell thicknesses and the GSND-II particles with various core sizes were confirmed by the high-resolution transmission electron microscope (HRTEM) analysis (Figure 2). Au core and Ag shell can be clearly distinguished from the images by the difference in contrast. The internanogap distance and silver shell thickness were determined from the HRTEM image analysis using the ImageJ software (rsb.info.nih.gov/ij). The Ag shell thickness of the GSND-I (denoted as d_{Ag1} and d_{Ag2} in Figure 2a) was varied from 5 to 8, 12, 16, 20, or 24 nm. As d_{Ag1} and d_{Ag2} get thicker, the internanogap distance was decreased from $\sim 4.8 \pm 2.7$ nm for $d_{Ag1} = d_{Ag2} = 5$ nm to $\sim 2.7 \pm 1.6$, $\sim 2.0 \pm 1.0$, $\sim 1.0 \pm 0.6$ and <1 nm for $d_{Ag1} = d_{Ag2} = 8$, 12, 16, and 20 nm, respectively. These are average values by analyzing 100 particles for each case (150 particles were analyzed for the 20-nm Ag shell cases that were targeted to generate <1 nm gap; Figure 2a3). It should be noted that there could be a slight discrepancy between the

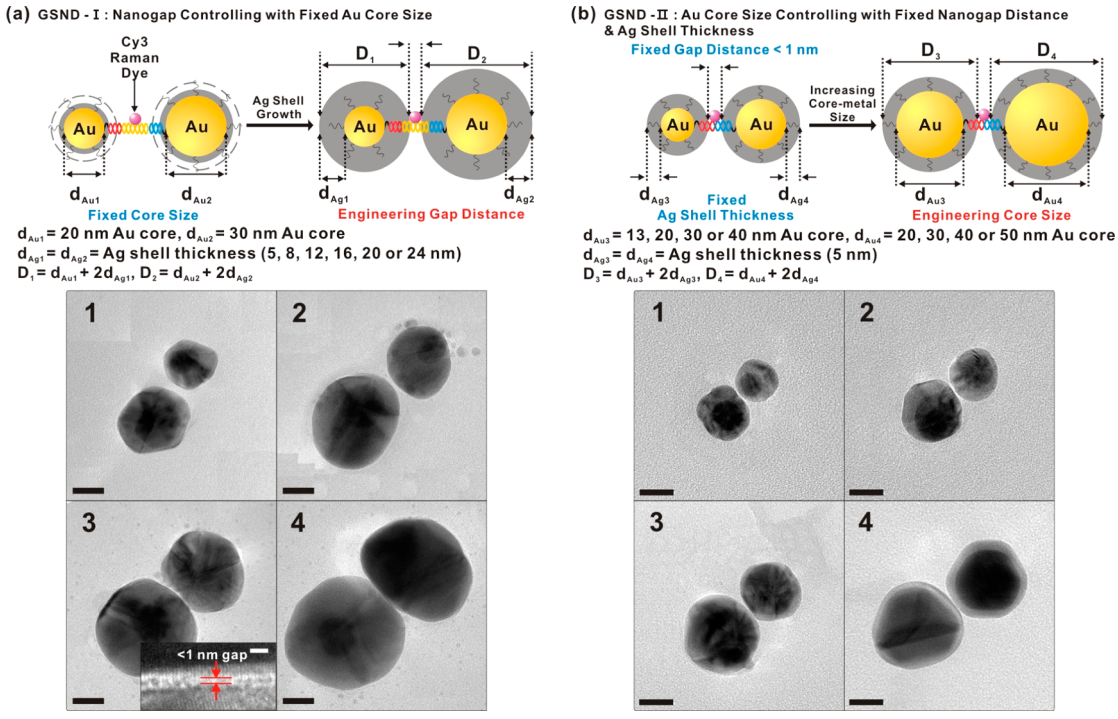

Figure 2. Gold−silver nanodumbbell (GSND) structures and corresponding HR-TEM images. The GSND-I was designed in a way that there is a plenty of space between AuNPs to generate GSND-I particles with various interparticle gap distances. The GSND-II was designed to have a fixed interparticle distance between two Ag surfaces while flexibly varying Au core size. The TEM images from a1 to a4 correspond to $d_{Ag1} = d_{Ag2}$ = 8 nm (a1), 16 nm (a2), 20 nm (a3), and 24 nm (a4), respectively. The images from b1 to b4 correspond to d_{Au3} = 13 nm/d_{Au4} = 20 nm (b1), d_{Au3} = 20 nm/d_{Au4} = 30 nm (b2), d_{Au3} = 30 nm/d_{Au4} = 40 nm (b3) and d_{Au3} = 40 nm/d_{Au4} = 50 nm (b4), respectively. All the scale bars are 20 nm (the scale bar in the inset image in Figure 2a3 is 1 nm).

actual gap sizes for the Raman and TEM measurements because the environments for the Raman (under air) and TEM (under vacuum) measurements, respectively, are different. The gap distance between dried particles under vacuum could be a bit shorter than that the distance between particles under air condition.[42] Further, for the particles with <1 nm gap, it is difficult to accurately measure the gap distance under 1 nm owing to the limitation in the HR-TEM resolution (~a few angstrom). For these reasons, we measured more particles than other cases to obtain a more reliable value and denoted the gap distance as <1 nm in this case. According to our measurements for <1 nm interparticle gap cases (the gap distance between one particle's lattice fringe and the other particle's lattice fringe; see the inset image in Figure 2a3), >97% of GSND-I particles have the gap distance of <1 nm. Due to the vacuum condition and limitation in resolution for the TEM measurement, we categorized all the particles with ~20 nm Ag shell into the GSND-I particles with <1 nm gap. Next, for the 24 nm Ag shell cases, no observable interparticle gap between particles was observed. For the fabrication of GSND-II particles with various Au core sizes, the Au core size of the dimeric pair (d_{Au3}−d_{Au4}) was varied (13−20 nm, 20−30 nm, 30−40 or 40−50 nm for universal probe core−probe B core). From the TEM analysis (Figure 2b), Ag shell thickness and the distance between particles were confirmed as ~5 nm and ~0.9 nm, respectively (average values were obtained by analyzing 100 particles for each case).

Controlling the internanogap distance and nanoparticle size in dimeric nanostructures is crucial in obtaining a large and controllable electromagnetic field enhancement for SERS.[38,42,45−48] To clarify the contribution of the interparticle distance-dependent SERS effect at single-molecule level, we performed the AFM-correlated nano-Raman experiments for single-particle analysis on the GSND-I. Since the focal laser spot (~300 nm) was precisely matched on the AFM-tip end, we were able to simultaneously image the GSND of interest and measure the SERS signal from the GSND. Figure 3b shows the AFM images of the GSND-I particles after spin-coating the particles on a poly-L-lysine-modified cover glass under ambient condition. The details for the measurement and calculation can be found in our previous literatures.[42,44] The UV−vis spectra for the GSND-I particles with varying Ag shell thickness are shown in Figure 3a. As the Ag shell grew, the UV−vis peak for AuNPs (~520 nm peak) started disappearing and the spectral feature for AgNPs (~450 nm peaks) appeared. For the thicker Ag shell, the UV−vis peak is red-shifted to a longer wavelength, and these results are in a good agreement with our previous results.[42] The AFM images along with the TEM analysis confirm that the size of the GSND-I and Ag

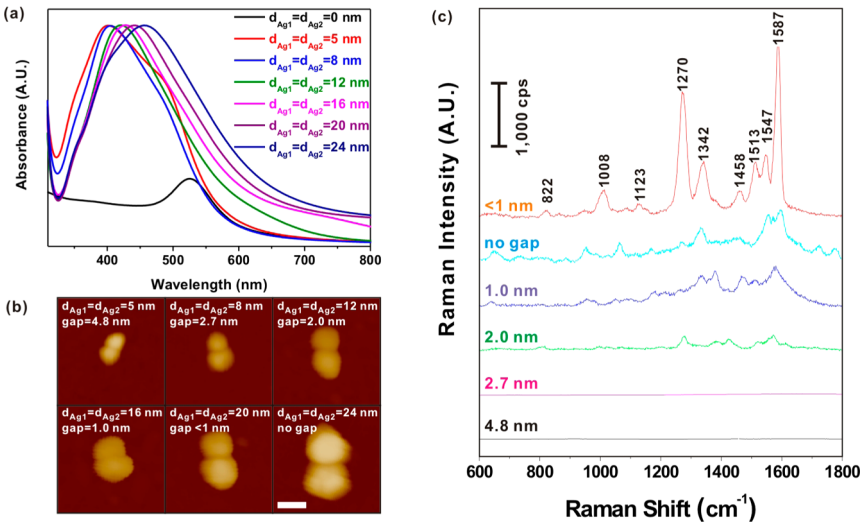

Figure 3. (a) The UV−vis spectra from interparticle-gap-controlled GSND-I structures with various Ag shell thicknesses and (b) AFM images of the GSND-I dimers obtained from the AFM-correlated nano-Raman measurement (scale bar = 50 nm). (c) Cy3 Raman spectra from the corresponding GSND-I structures (excitation = 514.5 nm, power = 100 μw, acquisition time = 1 s).

shell thickness are well controlled and highly correlated with interparticle gap distance (Figure 3b). All the SMSERS signals in Figure 3c were obtained with the following measurement condition −514.5 nm excitation laser, 100 μw laser power and 1 s acquisition time. When the interparticle gap was greater than ~2.7 nm, no SMSERS signal was detected. The SMSERS signal became weakly detectable when the gap distance was ~2.0 nm. In the case where the interparticle gap is ~1 nm, the SMSERS signal becomes clearly detectable with the characteristic Raman fingerprint peaks for Cy3 dye (1470 and 1580 cm^{-1}; Figure 3c). Importantly, when the gap is <1 nm, the SMSERS signal becomes much larger with much more distinct fingerprint peak features, and the Raman signals for 1470 and 1580 cm^{-1} were ~4.5 fold higher than the signal intensity for ~1 nm gap cases. It should be noted that the Raman signals in this case could typically last for *ca.* 1−2 min or up to 3−4 min in some occasions before photodamage, and these results are comparable to our previous results.[42] However, the SMSERS signal became much weaker when the interparticle gap was closed. The results show that keeping sub-1-nm gap distance is critical in generating strong SMSERS signals for the GSNDs. This trend is in good agreement with other reported results.[37,38,45,49]

Next, the SERS EFs were measured by averaging 50 measurements taken by 1 s acquisition time for each case using the AFM-correlated nano-Raman setup (for EF calculation, 1580 cm^{-1} peak was used). The average EF values as a function of the internanogap distance are shown in Figure 4a. Our data show a steep increase of EF value when the nanogap is <1 nm, and the overall trend agrees with other reported results.[37,38,45,49] The average maximum EF value at <1 nm gap distance (for d_{Ag1} = d_{Ag2} = 20 nm) was determined to be 1.8×10^{13} (the largest EF value was 5.9×10^{13}). This large enhancement could be partially attributed to the resonance[11,39,50] and chemical enhancement effects[51−55] along with strong electromagnetic field enhancement. The excitation wavelength for the electronic absorption of Cy3 (~550 nm) is close to the excitation laser wavelength (514.5 nm). It is known that the optimal resonance effect can occur when the laser excitation is matched with the absorption maximum of analytes, and the enhancement by this effect could be more than 1 order of magnitude.[11,39,50] The EF value rapidly dropped for the GSND with no gap (d_{Ag1} = d_{Ag2} = 24 nm), and it is likely that a Cy3 dye was embedded within Ag shell for the aggregated dimer; in this case, the dye was positioned inside the Ag shell. It should be noted that less reproducible SMSERS signals were observed in our previous results with the Au-nanobridged nanogap particles when a Raman dye was embedded in the Au shell.[44] Further, there has been intense research effort on understanding the plasmonic response of a dimer system with a very close interparticle proximity (<1 nm interparticle gap). In a dimer system, it is known that the red shift in the SPR band is typically observed while decreasing interparticle distance (hybridization of individual particle plasmons), but the blue shift in the SPR band is observed when conductive overlap or charge transfer plasmon starts to be present with increasing the overlap between two particles (single-particle-like plasmon).[56−59] Based on the quantum mechanical calculation, it was reported that particle hybridization and electromagnetic field enhancement resulted in the interaction between two plasmon resonances and this can be reduced by electron tunneling or charge transfer effect with decreasing the internanogap distance under 0.5 nm.[60] These results support our experimental results that the EF value was rapidly decreased and widely distributed for the GSNDs with no interparticle gap (d_{Ag1} = d_{Ag2} = 24 nm).

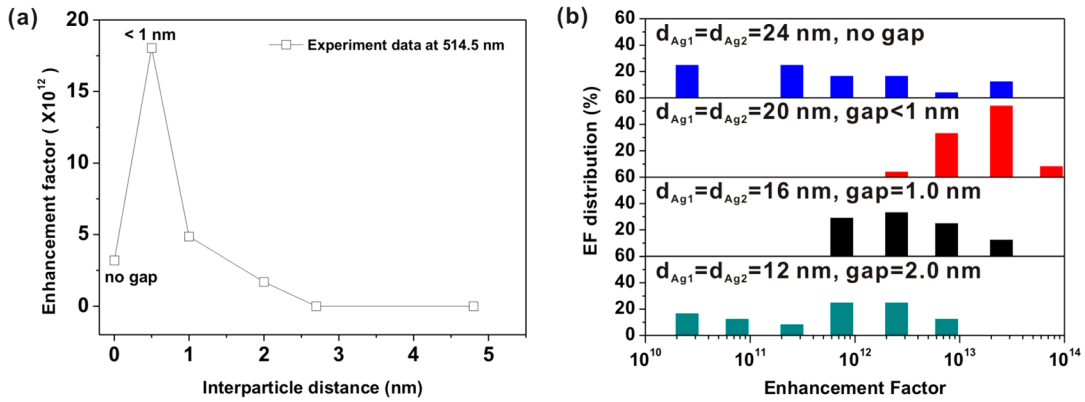

Figure 4. (a) The average enhancement factor values and (b) enhancement factor distributions for the GSND-I structures as a function of interparticle gap distance.

Next, we investigated the EF value distributions for various GSND-I particles (Figure 4b). In the EF value distribution graphs, we divided and categorized each order into two sections: 1−5 and 5−10. For example, we divided the EF values falling within 10^{10}−10^{11} into two groups: left section for the values between 1×10^{10} and 5×10^{10} and right section for the values between 5×10^{10} and 10^{11}. The EF value distributions are rather broad for the coalesced particles with no gap and the GSNDs with ∼2 nm gap. The narrowest distribution of high EF values was obtained for the GSNDs with <1 nm gap. We believe that this could be resulted from the structural reason. DNA is a polymer and has structural flexibility. If interparticle gap is large, it is more likely that a large part of a DNA strand can be exposed between two particles; in this case, DNA is not covered with Ag shell. It should be noticed that the exposed DNA part could be rotated and folded to create the structural flexibility and SERS signal uncertainties. As a result, it could have more diversity and freedom in DNA structure in the interparticle gap, which, in turn, creates more diverse EF values. On the contrary, when only a very small part of DNA is exposed between two particles, there is little freedom for the DNA to fluctuate within the junction and this can result in less diverse and more uniform EF values. In the case of the location of a Cy3 dye within the gap, a Cy3 is covalently modified to the phosphate backbone of a DNA. The Cy3 has a rotational degree of freedom due to its dangling configuration. It is quite possible that a Raman dye is not located at the shortest part of the junction, and it is highly likely that the molecule is located slightly off the center of the junction between two particles. Owing to the hot-spot localization effect and ultrasensitive change of SERS signal based on dye position and gap size, the standard deviation of enhancement factor distribution can be large for the SMSERS from the GSNDs.[61,62] These results strongly show that generating and controlling <1 nm interparticle gap is important not only for obtaining the strongest SERS signals but also for generating more stable and reproducible SERS signals.

To investigate the effect of Au core size on the SMSERS signal from the GSND systematically, we fixed the distance between particles and performed the SMSERS measurements using the AFM-correlated nano-Raman setup and 3D FEM calculations for the GSND-II structures (Figure 5). The GSND-II structures with different core sizes were characterized by monitoring changes in the UV−vis spectrum and solution color (Figure 5a). As the Au core size gets bigger and the relative volume of Au increases over that of Ag, solution color changes from yellow to reddish orange and ∼400 nm feature for AgNPs gets weaker. At the same time, ∼520 nm peak for AuNPs gets larger. It was recently reported that the plasmon resonances from bimetallic Au−Ag core−shell nanoparticles depend mainly on their relative sizes of the core and shell.[43] As the core−shell ratio is decreased from 1 to 0 (the volume of Au core is divided by the total volume of Au−Ag core−shell), which means increase in Ag shell thickness, the plasmon spectrum shows the influence of Ag shell as a blue shift, decrease of the low-energy plasmon resonance (>500 nm), and the appearance and increase of high-energy plasmon resonance (∼450 nm). These results indicate that the plasmon modes of core−shell nanoparticles strongly interact and cannot be viewed as additive individual contributions of core and shell modes. In our case, the volume ratio of core−shell is varied from ∼0.6 to ∼0.2, which corresponds to 40−50 nm and 13−20 nm Au cores, respectively. The reported results about the optical responses while changing the ratio between core and shell in core−shell nanoparticles are in a good agreement with our observations from the UV−vis spectrum and single-particle light-scattering spectrum (Figure 5a and the monomer spectrum in Figure 6). The corresponding AFM images further confirm that the GSND-II particles have been successfully synthesized with different core sizes. Next, the EF values were measured by the AFM-correlated nano-Raman method and calculated using the 3D FEM with two different excitation laser wavelengths (514.5 and 632.8 nm, respectively; Figure 5b). The SMSERS

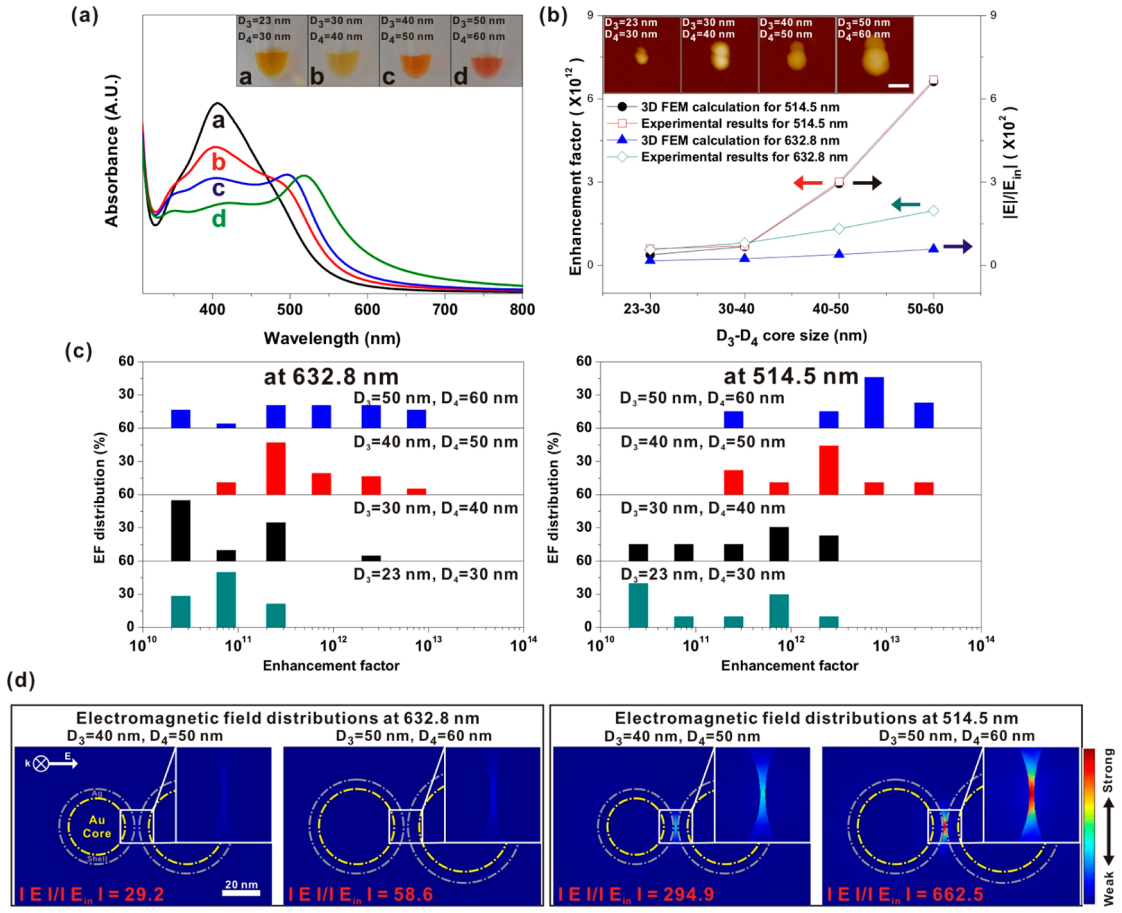

Figure 5. (a) The UV−vis spectra and corresponding solution color images (inset) for the GSND-II structures (Figure 2b1−4). (b) The experimental enhancement factor values and 3D FEM calculation results for GSND-II particles at two different excitation laser wavelengths of 514.5 nm (power = 100 μw and acquisition time = 1 s) and 632.8 nm (power = 140 μw and acquisition time = 1 s), respectively. The inset images show the corresponding AFM images (scale bar = 50 nm). (c) The enhancement factor distributions of GSND-II structures with 514.5 and 632.8 nm laser wavelengths. (d) 3D FEM-based electromagnetic field distributions with 514.5 and 632.8 nm laser wavelengths for 40−50 nm and 50−60 nm pairs. The results show that the field in the gap with 514.5 nm wavelength is much stronger than that with 632.8 nm wavelength.

signal by the AFM-correlated nano-Raman method became clearly stronger for 514.5 nm than 632.8 nm when Au core size got bigger than 40−50 nm and the trends in laser wavelength- and Au core size-dependence were in good agreement with the simulation results. The 3D FEM calculation and experimental results demonstrated that a larger Au core size with 514.5 nm laser generates a very high electromagnetic enhancement within the gap between particles, while much weaker plasmonic coupling was observed for the same Au core size with a 632.8 nm laser (Figure 5b−d). Additionally, a 514.5 nm excitation laser is closer to the excitation maximum wavelength (550 nm) of Cy3 dyes for inducing the effective resonance effect.[11,39,50] The contribution of the resonance effect along with other unknown effects, as we stated previously, can be estimated as >10 because the calculated result would correspond to around 1×10^{11} for $D_3-D_4 = 50-60$ nm. This effect could be one of the reasons why the experimentally obtained EF value with 514.5 nm excitation laser wavelength is higher than the EF value with 632.8 nm. The EF values with two different excitation laser wavelengths showed rather broad distributions with a ~0.9 nm interparticle gap (Figure 5c). This could result from the improper position of a Raman dye between particles as previously stated. It was reported elsewhere that the excitation laser wavelength for the SERS measurement should be carefully selected based on particle, size, shape, and composition because it can largely affect the resulting SERS signal.[63−65] Our results show not only that it is important to engineer the nanogap between particles but also that synthesizing the Au core and Ag shell with high precision in size and shape and choosing the appropriate excitation wavelength are critical in obtaining higher EF values with a narrow distribution. Furthermore, we found out that the relative volume between Au and Ag could affect their plasmon resonance energy due to the interaction between core and shell.

To further validate that our results with the GSND-I and GSND-II are based on the strong interaction

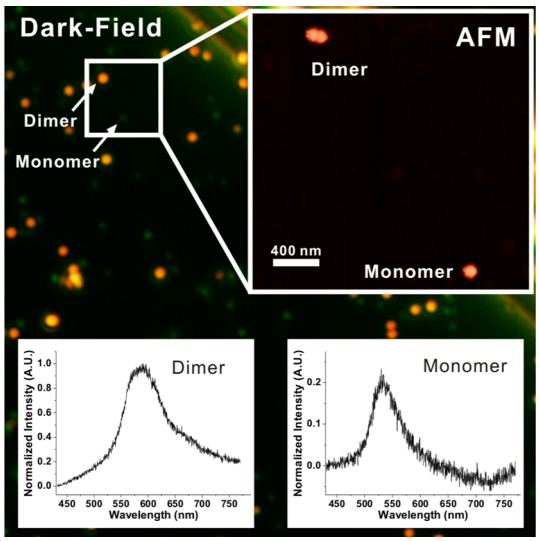

Figure 6. (a) The AFM-correlated dark-field scattering measurement for the GSND-II case with $D_3 = 50$ and $D_4 = 60$. The inset image shows the AFM image for the boxed area in the dark-field scattering image. The single-particle light-scattering spectra for the GSND-II dimer (left) and monomer (right) are also shown.

of two individual particles, single-particle scattering spectra were obtained using the AFM-correlated dark-field spectroscopy setup. Generally, the LSPR shoulder peak appears at the low-energy region for the dimer with a nanogap, which indicates the interaction between two particles.[45,48,64] However, it is not enough to show the interaction of two core−shell nanoparticles with our UV−vis results in Figures 3a and 5a because they are based on the ensemble-average data of monomers, dimers, and other multimers. For the Rayleigh light-scattering optical images and spectra at the single-particle level, the inverted microscope-based confocal system (NT-MDT, Russia) was used. Illumination was provided by a tungsten lamp through an oil-immersion dark-field condenser. Scattered light was collected by a 100× Plan Achromat objective (N.A. = 0.9, Olympus). The scattered light under the dark-field condition was then alternatively sent to the CCD camera (U-CMAD3, Olympus) or the confocal detection unit depending on selection of a beam path. The GSND-II with $D_3 = 50$ and $D_4 = 60$ was studied using this setup as a representative example. The results show that the maximum peak at 580−620 nm was obtained with higher signal intensity for the dimeric GSND-II, indicating the strong interaction between two core−shell nanoparticles, while the maximum peak around 520−530 nm was observed with lower intensity for the monomer (Figure 6). The larger SERS signals were observed with 514.5-nm laser than with 632.8-nm laser (Figure 5). However, one can notice that the resonance peak in Figure 6 is a bit closer to the 632.8-nm resonance than to the 514.5-nm resonance. Although the peak position of the surface plasmon resonance from the particles and illumination wavelength need to be matched for higher SERS signals, there are other important parameters that can play significant roles in generating stronger or weaker SERS signals. It was reported that the difference in the EF value was less than 1 order of magnitude when different illumination laser wavelengths were used with nonresonant dyes.[63] In our experiments, we used Cy3 dye, which is resonant with the excitation laser wavelength of 514 nm, to get more enhanced SERS signals. This effect can contribute up to $\sim 10^3$.[11,39] It is also known that the optical cross section of SERS is proportional to the fourth power of illumination laser wavenumber. By simple calculation, the 514-nm laser has ~2.3-fold larger optical cross section than 633-nm laser. In many cases, the illumination laser wavelength-dependent factor is less significant than the resonance effect and optical cross section.[66] These factors could result in the discrepancy between the surface plasmon absorption maximum peak and the electromagnetic field enhancement maximum peak.[67−69] Finally, it was further shown that the numerical calculation-based SERS enhancement spectrum could be less wavelength-dependent than the surface plasmon extinction spectrum.[66]

SUMMARY

We designed and synthesized two different dimeric GSND probe systems: the GSND-I that can systematically vary nanometer gap with the same Au core size and the GSND-II that can tune Au core size with a fixed subnanometer interparticle gap. With these two probe designs, along with the single-particle SERS measurement technique and 3D FEM calculation, we were able to systematically study the quantitative relationships between the plasmonic nanogap dimer structure and SMSERS signal with respect to the plasmonic coupling, SERS intensity, EF value distribution, and laser wavelength. By hybridization of target and filler DNA strands and subsequent Ag nanoshell formation, the interparticle distance within a GSND-I could be varied from ~4.8 nm to <1 nm or no gap. In this GSND-I design, we found out that <2 nm interparticle gap is needed to generate a detectable single-molecule SERS signal and <1 nm gap significantly boosts the SERS signal intensity while the SMSERS signal becomes much weaker when Au−Ag core−shell particles coalesce with no interparticle gap. Importantly, the EF value distribution results show that the GSNDs with <1 nm interparticle gap generated not only the strongest SMSER signals (the highest single EF value and the highest average EF value were 5.9×10^{13} and 1.8×10^{13}, respectively) but also the most narrow distribution of high EF values (EF values were distributed only between 1.9×10^{12} and 5.9×10^{13}). Meanwhile, the coalesced GSND-I particles with no interparticle gap and the GSND-I particles with 2.0 nm gap generated wide EF value distributions. In the GSND-II design, we could systematically vary Au core size from a 13−20 nm pair to a 40−50 nm pair

while fixing the Ag shell thickness at ~5 nm and interparticle gap distance at ~0.9 nm, respectively. Since the relative volume between Au and Ag could affect to their plasmon resonance energy, choosing a proper laser wavelength is key to generating higher and stronger SMSERS signals. Larger EF values for the GSND-II particles with larger Au cores from both experiments and 3D FEM simulation were observed for 514.5 nm excitation laser wavelength while this trend was less clear for 632.8 nm laser wavelength. The strategies shown here offer large flexibility and insight in designing and studying interparticle gap-based plasmonic coupling and the increased understanding of nanogap-based single-molecule SERS. Finally, the experimental and theoretical results in this study provide the evidence for the importance of engineering <1 nm gap between particles, and obtaining a narrow distribution of high EF values for more sensitive and quantitative SERS detection was heavily dependent on designing and synthesizing Au core and Ag shell with <1 nm level precision and coupling an appropriate excitation laser wavelength.

METHODS

Preparation of DNA-Modified AuNPs. DNA-modified AuNPs were synthesized and characterized based on literature procedures.[42,70] The reduced oligonucleotides by dithiothreitol (DTT, 0.1 M) in phosphate buffer (0.17 M, pH = 8.0) were purified using a desalting NAP-5 column. Futher purified oligonucleotides were mixed with AuNPs for the preparation of AuNP probes. For the preparation of universal probes, premixed universal probe DNA [5′-AAATAACAATAATCCCTC-PEG_{18}-A_{10}-$(CH_2)_3$-SH-3′] and universal protecting DNA [5′-CACGAGTTTCT-CAAA-PEG_{18}-A_{10}-$(CH_2)_3$-SH-3′] were conjugated to AuNPs. For the preparation of probe A, premixed probe A DNA without Cy3 [5′-HS-$(CH_2)_6$-A_{10}-PEG_{18}-ATCCTTATCAATATT-3′] and protecting DNA [5′-HS-$(CH_2)_6$-A10-PEG18-AAACTCTTTGAGCAC-3′] were conjugated to a different size of gold nanoparticles. For probe B, premixed probe B DNA with Cy3 [5′-HS-$(CH_2)_6$-A_{10}-PEG_{18}-ATCCTTATCAATATT-Cy3-3′] and protecting DNA [5′-HS-$(CH_2)_6$-A_{10}-PEG_{18}-AAACTCTTTGAGCAC-3′] were conjugated to AuNPs. The loading number of DNA was controlled stoichiometrically ([protecting DNA]/[probe DNA] = 69:1 for 13-nm AuNPs, 99:1 for 20-nm AuNPs, 199:1 for 30-nm AuNPs, 399:1 for 40-nm AuNPs, 799:1 for 50-nm AuNPs, respectively).[42,70] The excess amount of DNA (30-fold more) was added for all the probe modification processes. For details, please see the table in the Supporting Information. The mixtures were adjusted to obtain a final phosphate concentration of 10 mM (pH 7.4) with 100 mM phosphate buffer and a final concentration of 0.01% (wt/vol) SDS with 10% SDS. The resulting solution was wrapped in a foil and placed on an orbital shaker at room temperature for 60 min. Next, the mixtures were adjusted to 0.3 M NaCl (0.05 M × 2 and 0.1 M × 2) by the addition of salting buffer (2 M NaCl, 10 mM PB, 0.01% SDS) per every 20 min and heated for 5 min in a water bath at 70 °C after each step to minimize the interactions of DNA bases and gold surface.[70] After the salt-aging process, the solution was incubated overnight at room temperature. The solution was then centrifuged (10000 rpm for 13- and 20-nm AuNPs, 8000 rpm for 30- and 40-nm AuNPs and 6000 rpm for 50-nm AuNPs for 15 min, respectively) and the supernatant was removed. The precipitate was redispersed in 10 mM PB solution (pH 7.4; this procedure was repeated twice). Finally, the resulting particles were redispersed in a 0.3 M PBS and characterized using the UV−vis spectrophotometer (Agilent 8453 spectrophotometer, USA).

Preparation of Nanoparticle Dimers by DNA Hybridization. For the synthesis of the GSND-I particles, 6.5 μL of 1.07 nM DNA_U−AuNPs (20 nm AuNPs) and 23.5 μL of 0.30 nM DNA_A−AuNPs (30 nm AuNPs; a molar ratio of 1:1 for DNA_U−AuNP and DNA_A−AuNP) were mixed with 2.8 μL of 1 μM 61mer target DNA and 2.8 μL of 1 μM 31mer DNA_F with Cy3 dye (~400-fold higher concentration than probe concentration) in 0.3 M PBS solution. The mixtures were kept at >80 °C for 15 min to minimize nonspecific hybridization and then incubated on an orbital shaker at room temperature for 3−4 h. After centrifugation at 6000−8000 rpm for 10 min, the supernatant including unreacted target DNA was removed, and the precipitate was redispersed in 0.3 M PBS before the silver shell formation step. For the GSND-II synthesis, the same procedure was used with only shorter 30mer target DNA.

Silver Shell Formation. To control the interparticle nanogap distances by forming the Ag nanoshell, a chemical reduction method was used. 1% PVP, 0.1 M L-sodium ascorbate and 1 mM silver nitrate in deionized water were used to obtain a desired Ag shell thickness. (For varying Ag shell formations, please see the various silver shell formations section in the Supporting Information.) The molar ratio between the number of PVP repeating units and Ag^+ (PVP/Ag) was kept at 30 (the source for Ag^+ is $AgNO_3$), and the molar ratio between the number of PVP repeating units and reductant was kept at 15. For example, 37.3 μL of 1% PVP, 16.8 μL of 0.1 M L-sodium ascorbate and 111.9 μL of 1 mM silver nitrate were sequentially added to 30 μL of Au nanodumbell-I solution containing 6.5 μL of 1.07 nM DNA_U−AuNPs and 23.5 μL of 0.30 nM DNA_A−AuNPs for the formation of a 20 nm Ag shell. The resulting mixture was shaken and incubated overnight on the orbital shaker at room temperature. The solution was then centrifuged at 4000 rpm for 7 min for the GSND-I particles with 16, 20, or 24 nm Ag shell thickness and the GSND-II particles with d_{Au3}−d_{Au4} = 30−40 or 40−50 nm (5 nm Ag shell). For the GSND-I particles with 5-, 8- or 12-nm Ag shell thickness and the GSND-II particles with d_{Au3}−d_{Au4} = 13−20 or 30−40 nm (5 nm Ag shell), the solution was centrifuged at 6000 rpm for 10 min. After the centrifugation step to eliminate any unreacted residues, GSNDs were redispersed in 25 mM PBS solution. This GSND-I and GSND-II solution could be stored for 2−3 months before sampling for Raman measurement. After spin-coating the GSNDs on a poly-L-lysine-modified cover glass under ambient condition for Raman measurement, it should be used immediately for measurement since Ag oxidation will occur after 4−6 h after spin-coating.

Conflict of Interest: The authors declare no competing financial interest.

Supporting Information Available: Details for experimental methods, materials, and supporting figures. This material is available free of charge *via* the Internet at http://pubs.acs.org.

Acknowledgment. J.-M.N. was supported by the National Research Foundation of Korea (NRF) grant funded by the Korean government (MEST) (No. 2011-0018198) and POSCO (2011Y109). Y.D.S. was supported by KRICT (KK-0904-02, SI-1110), the Nano R&D Program (No. 2009-0082861), the Pioneer Research Center Program of NRF (No. 2009-0081511), the Development of Advanced Scientific Analysis Instrumentation Project of KRISS by MEST and the Eco-technopia 21 Project by KME. The authors would also like to acknowledge financial support from the Industrial Core Technology Development Program of the Ministry of Knowledge Economy (No. 10033183 and No. 10037397) and the KRICT OASIS Project from the Korea Research Institute of Chemical Technology.

REFERENCES AND NOTES

1. Nie, S.; Emory, S. R. Probing Single Molecules and Single Nanoparticles by Surface-Enhanced Raman Scattering. *Science* **1997**, *275*, 1102–1106.
2. Kneipp, K.; Wang, Y.; Kneipp, H.; Perelman, L. T.; Itzkan, I.; Dasari, R. R.; Feld, M. S. Single Molecule Detection Using Surface-Enhanced Raman Scattering (SERS). *Phys. Rev. Lett.* **1997**, *78*, 1667–1670.
3. Willets, K. A.; Van Duyne, R. P. Localized Surface Plasmon Resonance Spectroscopy and Sensing. *Annu. Rev. Phys. Chem.* **2007**, *58*, 267–297.
4. Moskovits, M. Surface-Enhanced Raman Spectroscopy: A Brief Retrospective. *J. Raman Spectrosc.* **2005**, *36*, 485–496.
5. Yonzon, C. R.; Zhang, X. Y.; Zhao, J.; Van Duyne, R. P. Surface-Enhanced Nanosensors. *Spectroscopy* **2007**, *22*, 42–55.
6. Krug, J. T., II; Wang, G. D.; Emory, S. R.; Nie, S. Efficient Raman Enhancement and Intermittent Light Emission Observed in Single Gold Nanocrystals. *J. Am. Chem. Soc.* **1999**, *121*, 9208–9214.
7. Cao, C. C.; Jin, R.; Mirkin, C. A. Nanoparticles with Raman Spectroscopic Fingerprints for DNA and RNA Detection. *Science* **2002**, *297*, 1536–1540.
8. Steven, E. J. B.; Narayana, M. S. S. Surface-Enhanced Raman Spectroscopy (SERS) for Sub-micromolar Detection of DNA/RNA Mononucleotides. *J. Am. Chem. Soc.* **2006**, *128*, 15580–15581.
9. Rodriguez-Lorenzo, L.; Alvarez-Puebla, R. A.; Pastoriza-Santos, I.; Mazzucco, S.; Stephan, O.; Kociak, M.; Liz-Marzan, L. M.; Garcia de Abajo, F. J. Zeptomol Detection through Controlled Ultrasensitive Surface-Enhanced Raman Scattering. *J. Am. Chem. Soc.* **2009**, *131*, 4616–4618.
10. Kneipp, K.; Kneipp, H.; Itzkan, I.; Dasari, R. R.; Feld, M. S. Surface-Enhanced Non-linear Raman Scattering at the Single-Molecule Level. *Chem. Phys.* **1999**, *247*, 155–162.
11. Dieringer, J. A.; Lettan, R. B.; Scheidt, K. A.; Van Duyne, R. P. A Frequency Domain Existence Proof of Single-Molecule Surface-Enhanced Raman Spectroscopy. *J. Am. Chem. Soc.* **2007**, *129*, 16249–16256.
12. Talley, C. E.; Jackson, B. J.; Oubre, C.; Grady, N. K.; Hollars, C. W.; Lane, S. M.; Huser, T. R.; Nordlander, P.; Halas, N. J. Surface-Enhanced Raman Scattering from Individual Au Nanoparticles and Nanoparticle Dimer Substrates. *Nano Lett.* **2005**, *5*, 1569–1574.
13. Nordlander, P.; Oubre, C.; Prodan, E.; Li, K; Stockman, M. Plasmon Hybridization in Nanoparticle Dimers. *Nano Lett.* **2004**, *4*, 899–903.
14. Garcia de Abajo, F. J. Nonlocal Effects in the Plasmons of Strongly Interacting Nanoparticles, Dimers, and Waveguides. *J. Phys. Chem. C.* **2008**, *112*, 17983–17987.
15. Sonnichsen, C.; Franzl, T.; Wilk, T.; Von Plessen, G.; Feldmann, J. Drastic Reduction of Plasmon Damping in Gold Nanorods. *Phys. Rev. Lett.* **2002**, *88*, 077402.
16. Jeanmaire, D. L.; Van Duyne, R. P. Surface Raman Spectroelectrochemistry: Part I. Heterocyclic, Aromatic, and Aliphatic Amines Adsorbed on the Anodized Silver Electrode. *J. Electroanal. Chem.* **1977**, *84*, 1–20.
17. Lee, S. J.; Morrill, A. R.; Moskovits, M. Hot Spots in Silver Nanowire Bundles for Surface-Enhanced Raman Spectroscopy. *J. Am. Chem. Soc.* **2006**, *128*, 2200–2201.
18. Romero, I.; Aizpurua, J.; Bryant, G. W.; F. Garcia de Abajo, J. Plasmons in Nearly Touching Metallic Nanoparticles: Singular Response in the Limit of Touching Dimers. *Opt. Express* **2006**, *14*, 9988–9999.
19. Fromm, D. P.; Sundaramurthy, A.; Schuck, P. J.; Kino, G.; Moerner, W. E. Gap-Dependent Optical Coupling of Single "Bowtie" Nanoantennas Resonant in the Visible. *Nano Lett.* **2004**, *4*, 957–961.
20. Xu, H.; Aizpurua, J.; Kall, M.; Apell, P. Electromagnetic Contributions to Single-Molecule Sensitivity in Surface-Enhanced Raman Scattering. *Phys. Rev. E* **2000**, *62*, 4318–4324.
21. Goulet, P. J. G.; Aroca, R. F. Distinguishing Individual Vibrational Fingerprints: Single-Molecule Surface-Enhanced Resonance Raman Scattering from One-to-One Binary Mixtures in Langmuir–Blodgett Monolayers. *Anal. Chem.* **2007**, *29*, 2728–2734.
22. Le Ru, E. C.; Blackie, E.; Meyer, M.; Etchegoin, P. G. Surface Enhanced Raman Scattering Enhancement Factors: A Comprehensive Study. *J. Phys. Chem. C* **2007**, *111*, 13794–13803.
23. Etchegoin, P. G.; Le Ru, E. C. A Perspective on Single Molecule SERS: Current Status and Future Challenges. *Phys. Chem. Chem. Phys.* **2008**, *10*, 6079–6089.
24. Park, W.–H.; Kim, Z. H. Charge Transfer Enhancement in the SERS of a Single Molecule. *Nano Lett.* **2010**, *10*, 4040–4048.
25. Michaels, A. M.; Jiang, J.; Brus, L. E. Ag Nanocrystal Junctions as the Site for Surface-Enhanced Raman Scattering of Single Rhodamine 6G Molecules. *J. Phys. Chem. B* **2000**, *104*, 11965–11971.
26. Larmour, I. A.; Faulds, K.; Graham, D. Improved Versatility of Silver Nanoparticle Dimers for Surface-Enhanced Raman Spectroscopy. *J. Phys. Chem. C* **2010**, *114*, 13249–13254.
27. Li, W.; Carmago, P. H. C.; Lu, X.; Xia, Y. Dimers of Silver Nanospheres: Facile Synthesis and Their Use as Hot Spots for Surface-Enhanced Raman Scattering. *Nano Lett.* **2009**, *9*, 485–490.
28. Novak, J. P.; Feldheim, D. L. Assembly of Phenylacetylene-Bridged Silver and Gold Nanoparticle Arrays. *J. Am. Chem. Soc.* **2000**, *122*, 3979–3980.
29. Sardar, R.; Heap, T. B.; Shumaker-Parry, J. S. Versatile Solid Phase Synthesis of Gold Nanoparticle Dimers Using an Asymmetric Functionalization Approach. *J. Am. Chem. Soc.* **2007**, *129*, 5356–5357.
30. Taylor, R. W.; Lee, T.-C; Scherman, O. A.; Esteban, R.; Aizpurua, J.; Huang, F. M.; Baumberg, J. J.; Mahajan, S. Precise Subnanometer Plasmonic Junctions for SERS within Gold Nanoparticle Assemblies Using Cucurbit[*n*]uril "Glue". *ACS Nano* **2011**, *5*, 3878–3887.
31. Wang, X.; Li, G.; Chen, T.; Yang, M.; Zhang, Z.; Wu, T.; Chen, H. Polymer-Encapsulated Gold-Nanoparticle Dimers: Facile Preparation and Catalytical Application in Guided Growth of Dimeric ZnO-Nanowires. *Nano Lett.* **2008**, *8*, 2643–2647.
32. Chen, G.; Wang, Y.; Yang, M.; Xu, J.; Goh, S. J.; Pan, M.; Chen, H. Measuring Ensemble-Averaged Surface-Enhanced Raman Scattering in the Hotspots of Colloidal Nanoparticle Dimers and Trimers. *J. Am. Chem. Soc.* **2010**, *132*, 3644–3645.
33. Loweth, C. J.; Caldwell, W. B.; Peng, X.; Alivisatos, A. P.; Schultz, P. G. DNA-Based Assembly of Gold Nanocrystals. *Angew. Chem., Int. Ed.* **1999**, *38*, 1808–1812.
34. Park, S. Y.; Lytton-Jean, A. K. R.; Lee, B.; Weigand, S.; Schatz, G. C.; Mirkin, C. A. DNA-Programmable Nanoparticle Crystallization. *Nature* **2008**, *451*, 553–556.
35. Li, W.; Camargo, P. H. C.; Au, L.; Zhang, Q.; Rycenga, M.; Xia, Y. Etching and Dimerization: A Simple and Versatile Route to Dimers of Silver Nanospheres with a Range of Sizes. *Angew. Chem., Int. Ed.* **2010**, *49*, 164–168.
36. Wang, Y.; Chen, G.; Yang, M.; Silber, G.; Xing, S.; Tan, L. H.; Wang, F.; Feng, Y.; Liu, X.; Li, S.; Chen, H. A Systems Approach towards the Stoichiometry-Controlled Heteroassembly of Nanoparticles. *Nat. Commun.* **2010**, *1*, 87.
37. Hill, R. T.; Mock, J. J.; Urzhumov, Y.; Sebba, D. S.; Oldenburg, S. J.; Chen, S. Y.; Lazarides, A. A.; Chilkoti, A.; Smith, D. R. Leveraging Nanoscale Plasmonic Modes To Achieve Reproducible Enhancement of Light. *Nano Lett.* **2010**, *10*, 4150–4154.
38. Zhu, W.; Banaee, M. G.; Wang, D.; Chu, Y.; Crozier, K. B. Lithographically Fabricated Optical Antennas with Gaps well below 10 nm. *Small* **2011**, *7*, 1761–1766.
39. Stokes, R. J.; Macaskill, A.; Lundahl, P. J.; Wmith, W. E.; Faulds, K.; Graham, D. Quantitative Enhanced Raman Scattering of Labeled DNA from Gold and Silver Nanoparticles. *Small* **2007**, *3*, 1593–1601.
40. Cao, Y. C.; Jin, R.; Mirkin, C. A. Nanoparticles with Raman Spectroscopic Fingerprints for DNA and RNA Detection. *Science* **2002**, *297*, 1536–1540.
41. Faulds, K.; Smith, W. E.; Graham, D. DNA Detection by Surface Enhanced Resonance Raman Scattering (SERRS). *Analyst* **2005**, *130*, 1125–1131.

42. Lim, D.−K.; Jeon, K.−S.; Kim, H. M.; Nam, J.−M.; Suh, Y. D. Nanogap-Engineerable Raman-Active Nanodumbbells for Single-Molecule Detection. *Nat. Mater.* **2010**, *9*, 60–67.
43. Chuntonov, L.; Bar-Sadan, M.; Houben, L.; Haran, G. Correlating Electron Tomography and Plasmon Spectroscopy of Single Noble Metal Core−Shell Nanoparticles. *Nano Lett.* **2012**, *12*, 145–150.
44. Lim, D.−K.; Jeon, K.−S.; Hwang, J.−H.; Kim, H. K.; Kwon, S. H.; Suh, Y. D.; Nam, J.−M. Highly Uniform and Reproducible Surface-Enhanced Raman Scattering from DNA-Tailorable Nanoparticles with 1-nm Interior Gap. *Nat. Nanotechnol.* **2011**, *6*, 452–460.
45. Hao, E.; Schatz, G. C. Electromagnetic Fields around Silver Nanoparticles and Dimers. *J. Chem. Phys.* **2004**, *120*, 357–366.
46. Wustholz, K. L.; Henry, A.−I.; Mcmahon, J. M.; Freeman, R. G.; Valley, N.; Piotti, M. E.; Natan, M. J.; Schatz, G. C.; Van Duyne, R. P. Structure−Activity Relationships in Gold Nanoparticle Dimers and Trimers for Surface-Enhanced Raman Spectroscopy. *J. Am. Chem. Soc.* **2010**, *132*, 10903–10910.
47. Hu, M.; Ou, F. S.; Wu, W.; Naumov, I.; Li, X.; Bratkovsky, A. M.; Williams, R. S.; Li, Z. Gold Nanofingers for Molecule Trapping and Detection. *J. Am. Chem. Soc.* **2010**, *132*, 12820–12822.
48. Li, W.; Camargo, P. H. C.; Lu, X.; Xia, Y. Dimers of Silver Nanospheres: Facile Synthesis and Their Use as Hot Spots for Surface-Enhanced Raman Scattering. *Nano Lett.* **2009**, *9*, 485–490.
49. Stiles, P. L.; Dieringer, J. A.; Shah, N. C.; Van Duyne, R. P. Surface-Enhanced Raman Spectroscopy. *Annu. Rev. Anal. Chem.* **2008**, *1*, 601–626.
50. Faulds, K.; Smith, W. E.; Graham, D. Evaluation of Surface-Enhanced Resonance Raman Scattering for Quantitative DNA Analysis. *Anal. Chem.* **2004**, *76*, 412–417.
51. Persson, B. N. J. On the Theory of Surface-Enhanced Raman Scattering. *Chem. Phys. Lett.* **1981**, *82*, 561–565.
52. Zhao, L.; Jensen, L.; Schatz, G. C. Pyridine−Ag20 Cluster: A Model System for Studying Surface-Enhanced Raman Scattering. *J. Am. Chem. Soc.* **2006**, *128*, 2911–2919.
53. Alexson, D. A.; Badescu, S. C.; Glembocki, O. J.; Prokes, S. M.; Rendell, R. W. Metal−Adsorbate Hybridized Electronic States and Their Impact on Surface Enhanced Raman Scattering. *Chem. Phys. Lett.* **2009**, *477*, 144–149.
54. Saikin, S. K.; Chu, Y.; Rappoport, D.; Crozier, K. B.; Aspuru-Guzik, A. J. Separation of Electromagnetic and Chemical Contributions to Surface-Enhanced Raman Spectra on Nanoengineered Plasmonic Substrates. *Phys. Chem. Lett.* **2010**, *1*, 2740–2746.
55. Shegai, T. O.; Haran, G. Probing the Raman Scattering Tensors of Individual Molecules. *J. Phys. Chem. B* **2006**, *110*, 2459–2461.
56. Atay, T.; Song, J. H.; Nurmikko, A. V. Strongly Interacting Plasmon Nanoparticle Pairs: From Dipole−Dipole Interaction to Conductively Coupled Regime. *Nano Lett.* **2004**, *4*, 1627–1631.
57. Romero, I.; Aizpurua, J.; Bryant, G. W.; de Abajo, F. J. G. Plasmons in Nearly Touching Metallic Nanoparticles: Singular Response in the Limit of Touching Dimers. *Opt. Express* **2006**, *14*, 9988–9999.
58. Lassiter, J. B.; Aizpurua, J.; Hernandez, L. I.; Brandl, D. W.; Romero, I.; Lal, S.; Hafner, J. H.; Nordlander, P.; Halas, N. Close Encounters between Two Nanoshells. *Nano Lett.* **2008**, *8*, 1212–1218.
59. de Abajo, F. J. G. Nonlocal Effects in the Plasmons of Strongly Interacting Nanoparticles, Dimers, and Waveguides. *J. Phys. Chem. C* **2008**, *112*, 17983–17987.
60. Zuloaga, J.; Prodan, E.; Nordlander, P. Quantum Description of the Plasmon Resonances of a Nanoparticle Dimer. *Nano Lett.* **2009**, *9*, 887–891.
61. EM Enhancements and Plasmon Resonances: Examples and Discussion. In *Principles of Surface-Enhanced Raman Spectroscopy and Related Plasmonic Effects*; Le Ru, E. C., Etchegoin, P. G., Eds.; Elsevier: Oxford, 2009; pp 299−364.
62. Le Ru, E. C.; Etchegoin, P. G.; Meyer, M. Enhancement Factor Distribution around a Single Surface-Enhanced Raman Scattering Hot Spot and Its Relation to Single Molecule Detection. *J. Chem. Phys.* **2006**, *125*, 204701.
63. Mcfarland, A. D.; Young, M. A.; Dieringer, J. A.; Van Duyne, R. P. Wavelength-Scanned Surface-Enhanced Raman Excitation Spectroscopy. *J. Phys. Chem. B* **2005**, *109*, 11279–11285.
64. Rycenga, M.; Hou, K. K.; Cobley, C. M.; Schwartz, A. G.; Camargo, P. H. C.; Xia, Y. Probing the Surface-Enhanced Raman Scattering Properties of Au−Ag Nanocages at Two Different Excitation Wavelengths. *Phys. Chem. Chem. Phys.* **2009**, *11*, 5903–5908.
65. Johnson, P.; Christy, R. Optical Constants of the Noble Metals. *Phys. Rev. B: Solid State* **1972**, *6*, 4370–4379.
66. Camden, J. P.; Dieringer, J. A.; Wang, Y.; Masiello, D. J.; Marks, L. D.; Schatz, G. C.; Van Duyne, R. P. Probing the Structure of Single-Molecule Surface-Enhanced Raman Scattering Hot Spots. *J. Am. Chem. Soc.* **2008**, *130*, 12616–12617.
67. Le Ru, E. C.; Galloway, C.; Etchegoin, P. G. On the Connection between Optical Absorption/Extinction and SERS Enhancements. *Phys. Chem. Chem. Phys.* **2006**, *8*, 3083–8087.
68. Tay, L.-L.; Hulse, J.; Kennedy, D.; Pezacki, J. P. Surface-Enhanced Raman and Resonant Rayleigh Scatterings from Adsorbate Saturated Nanoparticles. *J. Phys. Chem. C* **2010**, *114*, 7356–7363.
69. Jiang; Bosnick, K.; Maillard, M.; Brus, L. Single Molecule Raman Spectroscopy at the Junctions of Large Ag Nanocrystals. *J. Phys. Chem. B* **2003**, *107*, 9964–9972.
70. Hurst, S. J.; Lytton-Jean, A. K. R.; Mirkin, C. A. Maximizing DNA Loading on a Range of Gold Nanoparticle Sizes. *Anal. Chem.* **2006**, *78*, 8313–8318.